*Manuscript
Click here to view linked References

Nickel(II) complexes bearing a pincer ligand containing thioamide units : comparison between SNS and SCS pincer ligands.

Take-aki Koizumi,[a,*] Takuya Teratani,[a,b] Ken Okamoto,[a,b] Takakazu Yamamoto,[a] Yukihiro Shimoi,[c,d] Takaki Kanbara[b,e,*]

[a] *Chemical Resources Laboratory, Tokyo Institute of Technology, 4259 Nagatsuta, Midori-ku, Yokohama 226-8503, Japan*

[b] *Tsukuba Research Center for Interdisciplinary Materials Science (TIMS), University of Tsukuba, 1-1-1, Tennoudai, Tsukuba 305-8573, Japan*

[c] *Nanotechnology Research Institute, National Institute of Advanced Industrial Science and Technology (AIST), 1-1-1 Umezono, Tsukuba, Ibaraki 305-8568, Japan*

[d] *National Institute for Nanotechnology, National Research Council of Canada, 11421 Saskatchewan Drive, Edmonton, Albert, Canada T6G 2M9*

[e] *Graduate School of Pure and Applied Sciences, University of Tsukuba, 1-1-1, Tennoudai, Tsukuba 305-8573, Japan*

Abstract

Nickel(II) complexes bearing a κ^3SNS pincer ligand, 2,5-bis(benzylaminothiocarbonyl)pyrrolyl (**L1**) and a κ^3SCS pincer ligand, 2,6-bis(benzylaminothiocarbonyl)phenyl (**L2**), were synthesized, and their structures and electrochemical properties were elucidated. The crystal structures of [Ni(SNS)Br] (**2**) and [Ni(SCS)Br] (**5**) were determined by X-ray crystallography. The electrochemical and crystallographic data obtained from the complexes revealed that the κ^3SCS ligand has a stronger electron donating ability than the κ^3SNS ligand.

Keywords: Nickel / pincer complex / X-ray crystal structures / electron donating ability

1. Introduction

In recent years, nickel complexes bearing pincer ligands [1-6] have been widely investigated because of their interesting chemical properties. Many reports have been published on the electrochemical behavior of Ni-pincer complexes [2]. The strong electron-donating ability of the pincer ligand leads to a negative shift of the Ni(III)/Ni(II) redox potential [3]. However, most of the reported Ni pincer complexes have a benzene unit as a central aromatic ring of the pincer ligand. Recently, we have synthesized (κ^3SNS)-pincer complexes constructed of a pyrrole unit as a central aromatic ring and thioamide units as side arms as shown in Scheme 1 [4].

These complexes are stable in air, and the results of X-ray studies suggest that delocalization of the electrons occur through the central pyrrole ring and the thioamide group. Such a replacement of the central benzene unit by other aromatic or non-aromatic units modulates the chemical and electronic properties of the pincer complexes, and revealing the effect of modulation will be intriguing [3b,3d,5]. From the chemical and electrochemical viewpoints, the electronic properties of pincer complexes having a pyrrole unit as a central aromatic ring are considered to be different from those of benzene-centered pincer complexes. However, there have been no reports on the electrochemical properties of pyrrole-centered pincer complexes to the best of our knowledge. In this paper, we compared the SNS- and SCS-pincer ligand frameworks and elucidated the structure and electronic properties of their pincer nickel complexes.

2. Experimental

2.1 General, measurement, and materials.

^{1}H-NMR spectra were recorded on a JEOL Lambda-300 NMR spectrometer.

$^{13}C\{^{1}H\}$-NMR spectra were recorded on a JEOL JNM EX-400 NMR and Bruker TOPSPIN-400 spectrometer. IR spectra were recorded on a JASCO IR-810 spectrophotometer. UV-vis spectra were measured with a Shimadzu UV-2550 UV-visible spectrophotometer. Elemental analysis was carried out by the Center for Advanced Materials Analysis (Suzukakedai) in Tokyo Institute of Technology. Thermal analysis was performed with a Yanagimoto Seisakusho Micro Melting Point Apparatus. Electrochemical measurements were performed with a Hokuto Denko HSV-100 automatic polarization system. A conventional three-electrode configuration was used, with glassy carbon working (BAS electrode) and platinum wire auxiliary electrodes (Tokuriki, special order) and an Ag/0.1 M $AgNO_3$ reference (BAS RE-5). Cyclic voltammograms were recorded at a scan rate of 50 mV s^{-1}. Fc^{+}/Fc = +115 mV *vs*. 0.10 M $AgNO_3$/Ag, and +425 mV *vs*. SCE. *N*,*N*'-dibenzyl-1*H*-pyrrole-2,5-dicarbothioamide (**L1H**), *N*,*N*'-dibenzyl-benzene-1,3-dicarbothioamide (**L2H**), and [2,5-bis(benzylaminothiocarbonyl)pyrrolyl-κ^3N^1,S,S']chloronickel (**1**) were prepared according to the literature methods [4].

2.2. Synthesis and characterization

*2.2.1. [2,5-bis(benzylaminothiocarbonyl)pyrrolyl-κ^3N^1,S,S']bromonickel (**2**).*

$NiBr_2$ (43.7 mg, 0.20 mmol) and **L1H** (75.2 mg, 0.20 mmol) were dissolved in EtOH (5 mL) and stirred at room temperature for 24 h. The generated red precipitate was collected by filtration, washed with hexane, EtOH, and water, and dried in vacuo. (77.5 mg, 77% yield). mp: 148-150 ˚C (dec.). Anal. Calcd. for C20H18BrN3NiS2: C, 47.75; H, 3.61; N, 8.35%. Found: C, 47.45; H, 3.82; N, 8.13%. ^{1}H NMR (300 MHz, acetone-d_6): δ 10.14 (2H, s), 7.37 (10H, m), 6.57 (2H, s), 4.93 (4H, d, J = 6.7 Hz).

$^{13}C\{^{1}H\}$ NMR (100 MHz, acetone-d_6): δ 187.732, 144.997, 135.761, 128.747, 128.353, 128.050, 112.359, 50.391. FT-IR(KBr, cm^{-1}): 3280, 3086, 2957, 1558, 1496, 1390, 1344, 1261, 1180, 752, 418.

*2.2.2. [2,5-bis(benzylaminothiocarbonyl)pyrrolyl-κ^3N^1,S,S']iodonickel (**3**).*

The procedure for **2** was adopted using NiI_2 (31.3 mg, 0.1 mmol) to afford a red precipitate of **3** (42.0 mg, 77% yield). mp: 128-130 ˚C (dec.). Anal. Calcd. for C20H18IN3NiS2: C, 43.67; H, 3.3; N, 7.64%. Found: C, 42.81; H, 3.67; N, 7.03%. ^{1}H NMR (300 MHz, acetone-d_6): δ 10.15 (2H, s), 7.36 (10H, m), 6.67 (2H, d, J = 8.1 Hz), 4.93 (4H, d, J = 6.7 Hz). $^{13}C\{^{1}H\}$ NMR (100 MHz, acetone-d_6): δ 188.529, 144.616, 135.690, 128.764, 128.312, 128.076, 112.252, 50.513. FT-IR(KBr, cm^{-1}): 3289, 3248, 1653, 1387, 1348, 1263, 1240, 1055, 1028, 887, 744, 696.

*2.2.3. [2,6-Bis(benzylaminothiocarbonyl) -κ^2S,S'- phenyl-κC^1]chloronickel (**4**).*

$NiCl_2 \cdot 6H_2O$ (120 mg, 0.5 mmol) and **L2H** (188 mg, 0.5 mmol) were dissolved in toluene (5 mL) and stirred at 110 ˚C for 72 h. The precipitation were collected by filtration, washed with hexane and small amount of EtOH, and dried in vacuo to afford **4** as a red powder. (163 mg, 70% yield). mp: 120-125 ˚C (dec.). Anal. Calcd. for C22H19ClN2NiS2: C, 56.26; H, 4.08; N, 5.96%. Found: C, 55.90; H, 3.94; N, 5.71%. ^{1}H NMR (300 MHz, acetone-d_6): δ 10.13 (2H, s), 7.59 (2H, d, J = 7.7 Hz), 7.45 (4H, d, J = 7.1 Hz), 7.34 (6H, m), 7.03 (1H, t, J = 7.7 Hz), 5.04 (4H, d, J = 6.2 Hz). $^{13}C\{^{1}H\}$ NMR (100 MHz, DMSO-d_6): δ 197.9, 171.56, 146.71, 135.56, 128.34, 127.58, 127.42, 125.06, 121.42, 49.43 FT-IR(KBr, cm^{-1}): 3360, 3231, 1558, 1454, 1419, 1344, 1288, 1228, 1180, 1022, 924, 754, 733, 700.

*2.2.4. [2,6-Bis(benzylaminothiocarbonyl) -κ^2S,S'- phenyl-κC^1]bromonickel (**5**).*

The procedure for **4** was modified using $NiBr_2$ (43.7 mg, 0.2 mmol) to afford a red precipitate of **5** (54.5 mg, 53% yield). mp: 146-148 ˚C (dec.). Anal. Calcd. for C22H19BrN2NiS2: C, 51.39; H, 3.72; N, 5.45%. Found: C, 50.98; H, 4.18; N, 6.07%. ^{1}H NMR (300 MHz, acetone-d_6): δ 10.18 (2H, s), 7.67 (2H, d, J = 7.9 Hz), 7.50 (4H, d, J = 6.6 Hz), 7.36 (7H, m), 5.08 (4H, d, J = 6.1 Hz). ^{13}C{^{1}H} NMR (100 MHz, acetone-d_6): δ 198.816, 147.506, 136.290, 129.114, 128.325, 128.203, 125.763, 122.188, 50.083. FT-IR(KBr, cm^{-1}): 3362, 3225, 1651, 1553, 1495, 1454, 1290, 1184, 1024, 928, 797, 754, 700.

*2.2.5. [2,6-Bis(benzylaminothiocarbonyl) -κ^2S,S'- phenyl-κC^1]iodonickel (**6**).*

The procedure for **4** was modified using NiI_2 (31.25 mg, 0.1 mmol) to afford a red precipitate of **6** (42 mg, 77% yield). mp: 178-185 ˚C (dec.). Anal. Calcd. for C22H19IN2NiS2: C, 47.09; H, 3.41; N, 4.99%. Found: C, 46.61; H, 3.44; N, 4.91%. ^{1}H NMR (300 MHz, acetone-d_6): δ 10.23 (2H, s), 7.74 (2H, d, J = 8.0 Hz), 7.49 (2H, d, J = 7.9 Hz), 7.36 (8H, m), 7.11 (1H, t, J = 8.0 Hz), 5.08 (4H, d, J = 6.1 Hz). ^{13}C{^{1}H} NMR (100 MHz, acetone-d_6): δ 202.061, 147.244, 135.659, 128.704, 128.281, 127.963, 124.231, 121.929, 50.227. FT-IR(KBr, cm^{-1}): 3362, 3264, 1553, 1495, 1455, 1420, 1343, 1291, 1181, 1022, 922, 795, 739, 718, 698.

2.3. Crystal structure determination.

Crystals of **2** and **5** for X-ray analysis were obtained as described in the preparations. The crystal of **2** suitable for X-ray diffraction study was obtained by recrystallization from MeCN/EtOH and that of **5** was obtained from DMF. The suitable crystal was mounted on a glass fiber. Data collection for **2** and **5** was performed at -160 ˚C on a

Rigaku/MSC Saturn CCD diffractometer with graphite monochromated Mo-Kα radiation (λ = 0.7107 Å). The data were collected to a maximum 2θ value of 55°. A total of 720 oscillation images were collected. A sweep of data was done using ω scans from -110 ° to 70 ° in 0.5 ° steps, at χ = 45.0 ° and ϕ = 0.0 °. The structures were solved by using the CrystalStructure software package [7]. Atom scattering factors were obtained from the literature. Refinements were performed anisotropically for all non-hydrogen atoms by the full-matrix least-square method. Hydrogen atoms except for H1 and H2 were placed at the calculated positions and were included in the structure calculation without further refinement of the parameters. H1 and H2 of **2** and **5** were determined by difference Fourier map and refined isotropically. The residual electron densities were of no chemical significance. Crystal data and processing parameters are summarized in Table 6.

2.4. Computational Details.

All the TD-DFT calculations and natural population analysis (NPA) reported in this study were carried out using the Gaussian 03 suite of programs [8]. We employed the B3PW91 functional with LANL2DZ basis set implemented in Gaussian 03 programs suits. The molecular and crystal structures of all Ni pincer complexes derivative have been determined by X-ray diffraction were used for the NPA calculations. Geometry optimization for TD-DFT calculation was carried out under the constraint of *Cs* symmetry.

3. Results and discussion

3.1. Synthesis of Ni complexes.

The pincer ligand **L1H** [4] reacted with $NiCl_2$ in ethanol at room temperature to give the nickel-κ^3SNS pincer complex **1** with a 68% yield as shown in eq. 1. Similarly,

Br-complex **2** and I-complex **3** were obtained from the reaction of **L1H** with $NiBr_2$ and NiI_2, both with a 77% yield.

SCS-pincer Ni complexes **4-6** were prepared by the reaction of NiX_2 (X = Cl, Br, I) with **L2H** in toluene as shown in eq. 2.

All complexes, **1**-**6**, were characterized by IR and ^{1}H-NMR spectroscopy. In the ^{1}H-NMR spectra of **1**, **2**, and **3**, a broadened N-H resonance of the thioamide group appeared at δ 10.09, 10.14, and 10.15, respectively. The peak was shifted to a lower magnetic field from that of **L1H** (δ 8.98) by 1.11-1.17 ppm. The resonance of the pyrrole N-H proton in **L1H** (δ 10.62) reasonably disappeared for **1**-**3**. On the other hand, in the ^{1}H-NMR spectra of **4**-**6**, the resonance based on the N-H in the thioamide group appeared at δ 10.13, 10.18, and 10.23, respectively. They were also shifted to a lower magnetic field from that of the N-H (thioamide) signal of **L2H**.

*3.2. Molecular structures of Ni **2** and **5**.*

Fig. 1 and 2 depict the molecular structures of **2** and **5**, respectively, determined by X-ray crystallography, and selected bond lengths and angles of the complexes are summarized in Tables 1 and 2, respectively. **2** and **5** have an almost planar structure; the sum of the bond angles around the Ni center of **2** and **5** are 359.98° and 360.00°, respectively. The Ni1-C1 bond length in **5** is 1.8630(11) Å, which is similar or longer than those in benzene-centered Ni(II)-NCN pincer complexes (1.814(2)-1.859(4) Å) [2a,9], and shorter than those in benzene-centered PCP pincer complexes (1.879(2)-1.931(2) Å) [3b, 3d, 10]. The Ni1-Br1 bond length in **2** is 2.321(2) Å, which is shorter than that in **5** (2.3686(2) Å); this is due to the *trans* influence of the benzene unit is more significant than that of the pyrrole unit.

In the IR spectra, the ν(N-H) band of **1**-**3** was observed as a shoulder peak at about

3300 cm^{-1}. On the other hand, the ν(N-H) peaks of **4**-**6** were clearly observed at 3360-3362 cm^{-1}. As mentioned above, **L1** in **2** has an electron-delocalized resonance structure as shown in Scheme 2 [4]. The electronic structure appears to give a lower shift of the wavenumber of the ν(N-H) band in complexes **1**-**3**.

The X-ray crystallographic data of **2** reveal that it contains solvated acetonitrile in the crystal state. The two N-H protons in **2** undergo on intermolecular interaction with other molecules. One N-H proton in **2** is positioned near the Br atom in the neighboring Ni complex (N-H···Br, 2.67(11) Å), and the other N-H proton interacts with the N atom in solvated acetonitrile (N-H···N, 2.09(15) Å). Fig. 3(a) shows the packing structure of **2**·MeCN. As shown in Fig. 3(a), **2**·MeCN forms an alternating network by hydrogen bonding. The N-H hydrogens of **5**·DMF also undergo intermolecular interactions. As depicted in Fig. 3(b), one of the N-H hydrogen atoms interacts with the Br atom in the neighboring molecule with an Ni-Br···H-N distance of 2.750(15) Å. The other N-H hydrogen interacts with solvated DMF with a C=O···H-N distance of 1.909(13) Å. **2**·MeCN and **5**·DMF, have different packing structures form each other. The packing structure of **2**·MeCN is similar to that of the previously reported **1**·MeCN [4], and **5**·DMF has a packing structure similar to that of a DMF-solvated SCS-Ni-Cl complex [6b].

The electronic spectra of **2** and **5** are shown in Fig. 4, and the spectral data of **1**-**6** are summarized in Table 3. **1**-**3** exhibit intense absorption bands at λ_{max} = 286-292 and 369-372 nm, which are assigned to the π–π* transitions in the SNS pincer ligand. Weak absorption is observed in the region of 390-420 nm, which can be assigned to a metal-to-ligand charge transfer (MLCT) band [7]. In **4**-**6**, a significant MLCT band is observed at λ_{max} = 440–452 nm, whose intensities are stronger than those of **1**-**3**. The assignments of the π–π* transition and the MLCT absorption bands were examined by

time-dependent density functional theory (TD-DFT) calculations (Table 4) on isolated complexes. Three-dimensional plots of the HOMOs and LUMOs of **2** and **5**, and their molecular orbitals (MO) are depicted in Fig. 5 using GaussView 4.1 [12]. From the results of the TD-DFT calculation, **2** has a relatively weak absorption at 506 nm that is dominated by a transition from HOMO to LUMO. On the other hand, **5** has two stronger transitions in the MLCT band originating from HOMO -2 to LUMO and HOMO -4 to LUMO. These occupied levels possess a certain amount of weight at the d orbitals of the nickel atom and the π orbitals of the ligand, respectively, and the LUMOs possess a strong ligand character.

3.3. Electrochemical and optical data of the Ni complexes.

Cyclic voltammograms (CVs) of **1**-**6** were recorded in DMF solution containing 0.10 M $[N(n\text{-}Bu)_4]PF_6$ as the supporting electrolyte using a glassy carbon working electrode. The CVs of **1** and **4** in the region of -0.3 to +0.5 V are displayed in Fig. 6, and the electrochemical data of complexes **1**-**6** are summarized in Table 5. In the region as shown in Fig.6, **1** exhibits a quasi-reversible wave based on the Ni(III)/Ni(II) redox couple [13] at $E_{1/2}$ = +0.336 V (*vs* Fc^+/Fc). The $E_{1/2}$ value of the Ni(III)/Ni(II) redox couple of **4** is observed at +0.055 V (*vs* Fc^+/Fc). The occurrence of a much facile oxidation of **4** than that of **1** suggests a higher electron-donating ability of **L2** to Ni than that of **L1**. A similar tendency is also observed for other couples of complexes (**2** *vs* **5** and **3** *vs* **6**, Table 5). These results are consistent with the X-ray crystallographic and electronic spectral data. In almost all cases, many of the Ni-pincer complexes exhibited an irreversible oxidative wave in a more positive region, suggesting the formation of higher oxidized Ni species or oxidation of the thioamide ligand, however, the formed species have not been identified.

The DFT calculation also suggests the higher electron donating ability of **L2** than that of **L1**. The contour plots of the HOMOs of **2** and **5** are shown in Fig. 6. The HOMO level of **2** (-0.208 eV) is slightly deeper than that of **5** (-0.197 eV). We have also calculated the electron densities of **2** and **5** using a DFT method. The atomic charges were estimated by natural population analysis (NPA) [14], which is well known to be less dependent on the basis set than Mulliken population analysis. The NPA charges of **2** and **5** are shown in Fig. 7. These results indicate that the natural charge of the nickel atom of **2** is more positive than that of **5**, which is consistent with the results of X-ray crystallography study and cyclic voltammetry.

4. Conclusion

We have elucidated the synthesis, structures, and electrochemical properties of Ni-SNS and Ni-SCS pincer complexes. The pincer ligands smoothly coordinate to Ni in a tridentate fashion *via* a cyclometalation process. The Ni(III)/Ni(II) redox potentials of complexes **1-6** are significantly influenced by the electronic effects of the N- and C-σ-bonded unit in the pincer ligand. The X-ray crystallography of **2** and **5** indicated that the *trans* influence of **L2** is larger than that of **L1**. These results reveal that the centered benzene unit of **L2** has a higher electron donating capability to the metal center than centered pyrrole unit of **L1**. These findings are expected to contribute to the modulation of chemical properties of the pincer complexes.

5. Supplementary materials

Crystallographic data for the structural analysis of **2**, and **5** in CIF format have been deposited with the Cambridge Crystallographic Data Centre under CCDC No. 707890 (**2**) and 707891 (**5**), respectively. These data can be obtained free of charge via www.ccdc.cam.ac.uk/conts/retrieving.html (or from the CCDC, 12 Union Road, Cambridge CB2 1EZ, UK; fax: +44 1223 336033; e-mail: deposit@ccdc.cam.ac.uk).

Acknowledgement

Y.S. acknowledges partial financial support from the Grant-in-Aid for Science Research in a Priority Area “Super-Hierarchical Structures” (17067018) from the Ministry of Education, Culture, Sports, Science and Technology of Japan.

*Corresponding author. Tel: +81-45-924-5222; fax: +81-45-924-5976.

E-mail: tkoizumi@res.titech.ac.jp (T. Koizumi)

References

[1] For reviews, see: (a) R.A. Gossage, L.A. van de Kuil, G. van Koten, Acc. Chem. Res. 31 (1998) 423; (b) J.T. Singleton, Tetrahedron, 59 (2003) 1837; (c) H. Nishiyama, Chem. Soc. Rev. 36 (2007) 1133.

[2] For examples, see: (a) D.M. Grove, G. van Koten, R. Zoet, J. Am. Chem. Soc. 105 (1983) 1379; (b) L.A. van de Kuil, H. Luitjes, D.M. Grove, J.W. Zwikker, J.G.M. van der Linden, A.M. Roelofsen, L.W. Jenneskens, W. Drenth, G. van Koten, Organometallics 13 (1994) 468.

[3] (a) D.M. Grove, G. van Koten, P. Mul, R. Zoet, J.G.M. Van der Linden, J. Legters, J.E.J. Schmitz, N.W. Murrall, A.J. Welch, Inorg. Chem. 27 (1988) 2466; (b) V. Pandarus, D. Zargarian, Chem. Commun. (2007) 978; (c) M. Stol, D.J. M. Snelders, M.D. Godbole, R.W.A. Havenith, D. Haddleton, G. Clarkson, M. Lutz, A.L. Spek, G.P.M. van Klink, G. van Koten, Organometallics 26 (2007) 3985; (d) V. Pandarus, D. Zargarian, Organometallics 26 (2007) 4321.

[4] K. Okamoto, T. Kanbara, T. Yamamoto, Chem. Lett. 35 (2006) 558.

[5] a) O.V. Ozerov, C.Guo, L. Fan, B.M. Foxman, Organometallics 23 (2004) 5573; (b) A. Castonguay, C. Sui-Seng, D. Zargarian, A.L. Beauchamp, Organometallics 25 (2006) 602; (c) L.-C. Liang, P.-S. Chien, J.-M. Lin, M.-H. Huang, Y.-L. Huang, J.-H. Liao, Organometallics 25 (2006) 1399; (d) L. –C. Liang, P. –S. Chien, Y. -L. Huang, J. Am. Chem. Soc. 128 (2006) 15562; (e) W. Li, Z. –X. Wang, Org. Lett. 9 (2007) 4335; (f) J.C. DeMott, F. Basuli, U.J. Kilgore, B.M. Foxman, J.C. Huffman, O.V. Ozerov, D.J. Mindiola, Inorg. Chem. 46 (2007) 6271; (g) H. Meguro, T. Koizumi, T. Yamamoto, T. Kanbara, J. Orgnomet. Chem. 693 (2008) 1109; (h) G.W. Bates, P.A. Gale, M.E. Light, M.I. Ogden, C.N. Warriner, Dalton Trans. (2008) 4106.

[6] a) K. Okamoto, T. Yamamoto, T. Kanbara, J. Nanosci. Nanotechnol. 9 (2009) 646;

(b) K. Okamoto, Ph. D. Thesis, Tokyo Institute of Technology, 2008.

[7] *Crystal Structure*: Crystal Analysis Package, Rigaku and Rigaku/MSC, 2000-2006.

[8] a) Gaussian 03, Revision D.01, M. J. Frisch, G.W. Trucks, H.B. Schlegel, G.E. Scuseria, M.A. Robb, J.R. Cheeseman, J.A. Montgomery, Jr., T. Vreven, K.N. Kudin, J.C. Burant, J.M. Millam, S.S. Iyengar, J. Tomasi, V. Barone, B. Mennucci, M. Cossi, G. Scalmani, N. Rega, G.A. Petersson, H. Nakatsuji, M. Hada, M. Ehara, K. Toyota, R. Fukuda, J. Hasegawa, M. Ishida, T. Nakajima, Y. Honda, O. Kitao, H. Nakai, M. Klene, X. Li, J.E. Knox, H.P. Hratchian, J.B. Cross, V. Bakken, C. Adamo, J. Jaramillo, R. Gomperts, R.E. Stratmann, O. Yazyev, A.J. Austin, R. Cammi, C. Pomelli, J.W. Ochterski, P.Y. Ayala, K. Morokuma, G.A. Voth, P. Salvador, J.J. Dannenberg, V.G. Zakrzewski, S. Dapprich, A.D. Daniels, M.C. Strain, O. Farkas, D.K. Malick, A.D. Rabuck, K. Raghavachari, J.B. Foresman, J.V. Ortiz, Q. Cui, A.G. Baboul, S. Clifford, J. Cioslowski, B.B. Stefanov, G. Liu, A. Liashenko, P. Piskorz, I. Komaromi, R.L. Martin, D.J. Fox, T. Keith, M.A. Al-Laham, C.Y. Peng, A. Nanayakkara, M. Challacombe, P.M.W. Gill, B. Johnson, W. Chen, M.W. Wong, C. Gonzalez, and J.A. Pople, Gaussian, Inc., Wallingford CT (2004); (b) J.P. Foster, F. Weinhold, J. Am. Chem. Soc. 102 (1980) 7211; (c) E.D. Glendening, A.E. Reed, J.E. Carpenter, F. Weinhold, NBO Version 3.1.

[9] (a) D.M. Grove, G. van Koten, H.J.C. Ubbels, R. Zoet, Organometalics 3 (1984) 1003; (b) D.M. Grove, G. van Koten, W.P. Mul, A.A.H. van der Zeijden, J. Terheijden, Organometallics 5 (1986) 322; (c) J.A.M. van Beek, G. van Koten, M.J. Ramp, N.C. Coenjaarts, D.M. Grove, K. Goubitz, M.C. Zoutberg, C.H. Stam, W.J.J. Smeets, A.L. Spek, Inorg. Chem. 30 (1991) 3059.

[10] M.E. van der Boom, S.-Y. Liou, L.J.W. Shimon, Y. Ben-David, D. Milstein,

Inorg chim, Acta 357 (2004) 4015; (b) J. Capora, P. Palma, D. del Rio, E. Alvarez, Organometallics 23 (2004) 1652; (c) J. Capora, P. Palma, D. del Rio, M.M. Conejo, E. Alvarez, Organometallics 23 (2004) 5653; (d) D. Benito-Garagorri, V Bocokie, K Mereiter, K. Kirchner, Organometallics 25 (2006) 3817.

[11] The MLCT absorption band of Ni-pincer complexes has been discussed previously; L.A. van de Kuil, D.M. Grove, J.W. Zwikker, L.W. Jenneskens, W. Drenth, G. van Koten, Chem. Mater. 6 (1994) 1675.

[12] GaussView, Version 4.1, Roy Dennington II, Todd Keith and John Millam, Semichem, Inc., Shawnee Mission, KS, 2007.

[13] G. van Koten *et al*. reported the CV of Ni-NCN complexes, and they assigned the quasi-reversible redox wave observed at about $E_{1/2}$ = 0.14 V (*vs*. Ag/AgCl) to the Ni(II)/Ni(III) redox couple [3a]. Thioaides **L1H** and **L2H** did not show the oxidized peak in the region of -0.4 to + 0.5 V in CV.

[14] A.E. Reed, R.B. Weinstock, F. Weinhold, J. Chem. Phys. 83 (1985) 735.

Captions

Fig. 1. ORTEP drawing of **2**·MeCN with 50% ellipsoidal level. Hydrogen atoms except for H1 and H2 and solvated MeCN molecules are omitted for clarity.

Fig. 2. ORTEP drawing of **5**·DMF with 50% ellipsoidal level. Hydrogen atoms except for H1 and H2 and solvated DMF molecules are omitted for clarity.

Fig. 3. Packing diagrams of (a) **2**·MeCN and (b) **5**·DMF.

Fig. 4. Electronic spectra of (a) **2** and (b) **5** in MeCN.

Fig. 5. Molecular orbitals (MO) and their levels of (a) **2** and (b) **5** calculated at the B3PW91/LANL2-DZ level, respectively.

Fig. 6. Cyclic voltammograms of (a) **1** and (b) **4** in MeCN; 0.10 M $[N(n\text{-}Bu)_4]PF_6$, scan rate 50 mVs^{-1}, glassy carbon working electrode.

Fig. 7. Natural charge of (a) **2** and (b) **5** calculated by NPA.

Scheme 1. Molecular structure of the M-(κ^3SNS) complex.

Scheme 2. Delocalization of electrons in the Ni(SNS) complex.

Table 1. Selected bond lengths (Å) and angles (°) of 2·MeCN.

Table 2. Selected bond lengths (Å) and angles (°) of 5·DMF.

Table 3. UV-vis spectral data for the complexes in MeCN.

Table 4. Selected Calculated Singlet Excited-State Transitions for Complexes for 2 and 5.

Table 5. Electrochemical data for complexes 1-6.

Table 6. Crystal data and details of the structure refinement of 2·MeCN and 5·DMF.

***Graphical abstract (synopsis)**

Graphical abstract

Nickel(II) complexes bearing a pincer ligand containing thioamide units : comparison between SNS and SCS pincer ligands

Take-aki Koizumi,* Takuya Teratani, Ken Okamoto, Takakazu Yamamoto, Takaki Kanbara,* and Yukihiro Shimoi

Two types of pincer nickel(II) complexes bearing a κ^3SNS pincer ligand and a κ^3SCS pincer ligand were synthesized, and their electrochemical properties were elucidated. Electrochemical data of the complexes revealed that the κ^3SCS ligand had a stronger electron donating ability than the κ^3SNS ligand.

Graphical Abstract (pictogram)

Click here to download high resolution image

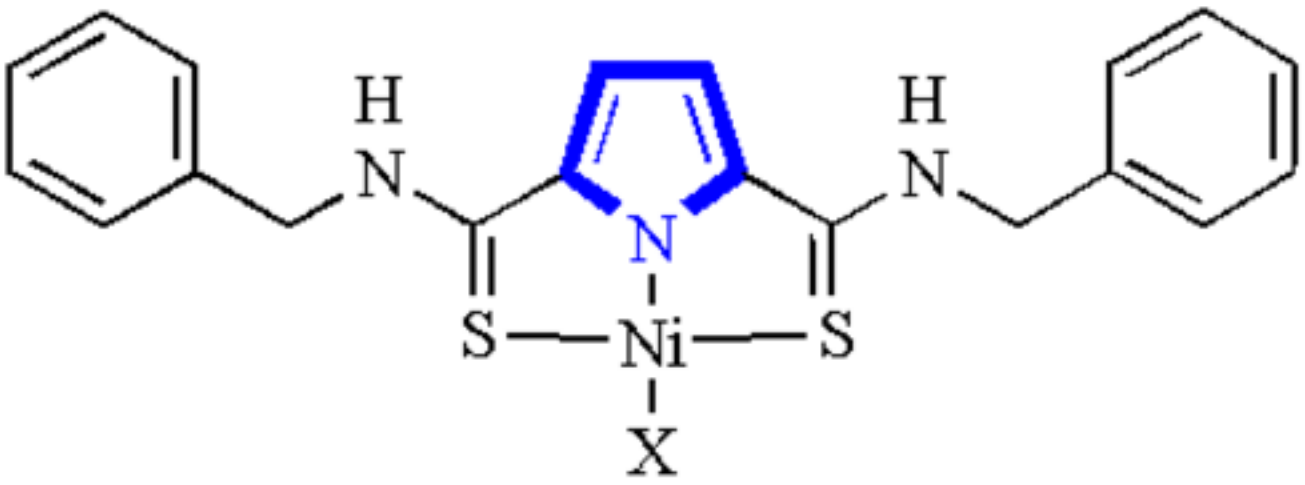

SNS-Ni-X

vs. X = Cl, Br, I

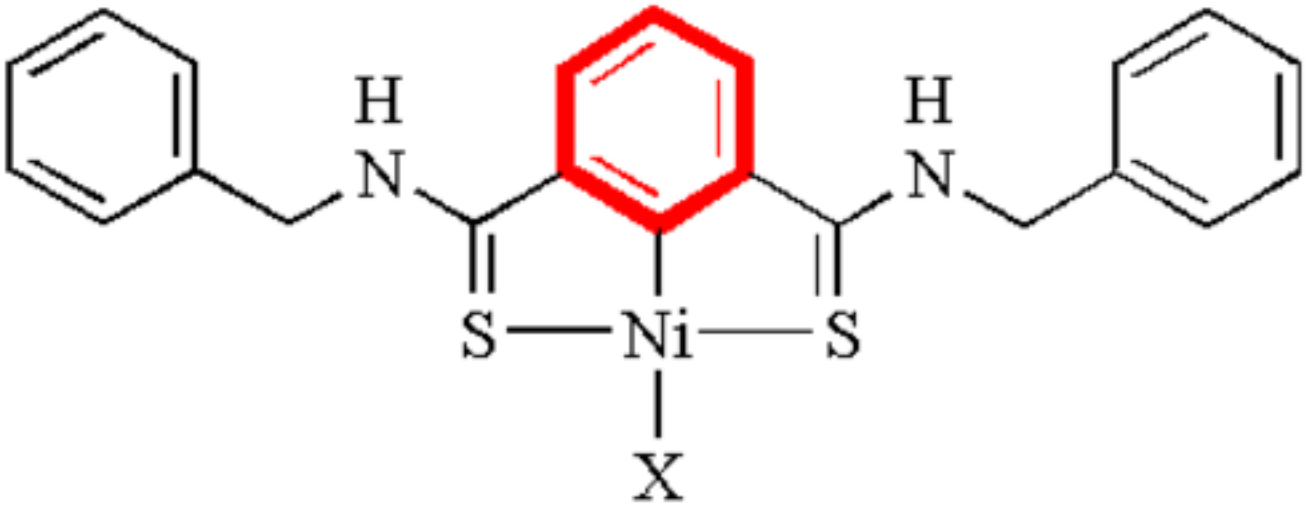

SCS-Ni-X

Figure(s)
Click here to download high resolution image

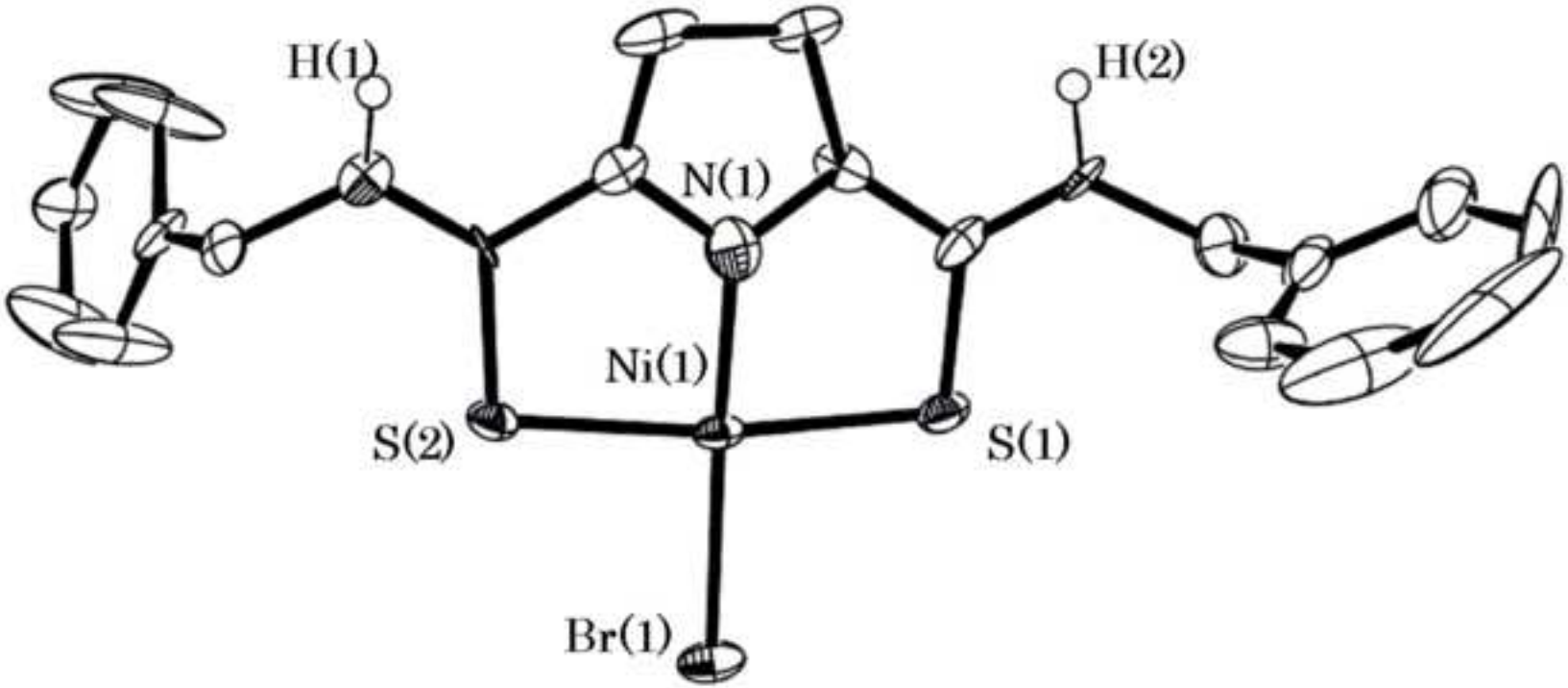

Fig. 1. ORTEP drawing of **2** MeCN with 50% ellipsoidal level. Hydrogen atoms except for H1 and H2 and solvated MeCN molecules are omitted for clarity.

Figure(s)
Click here to download high resolution image

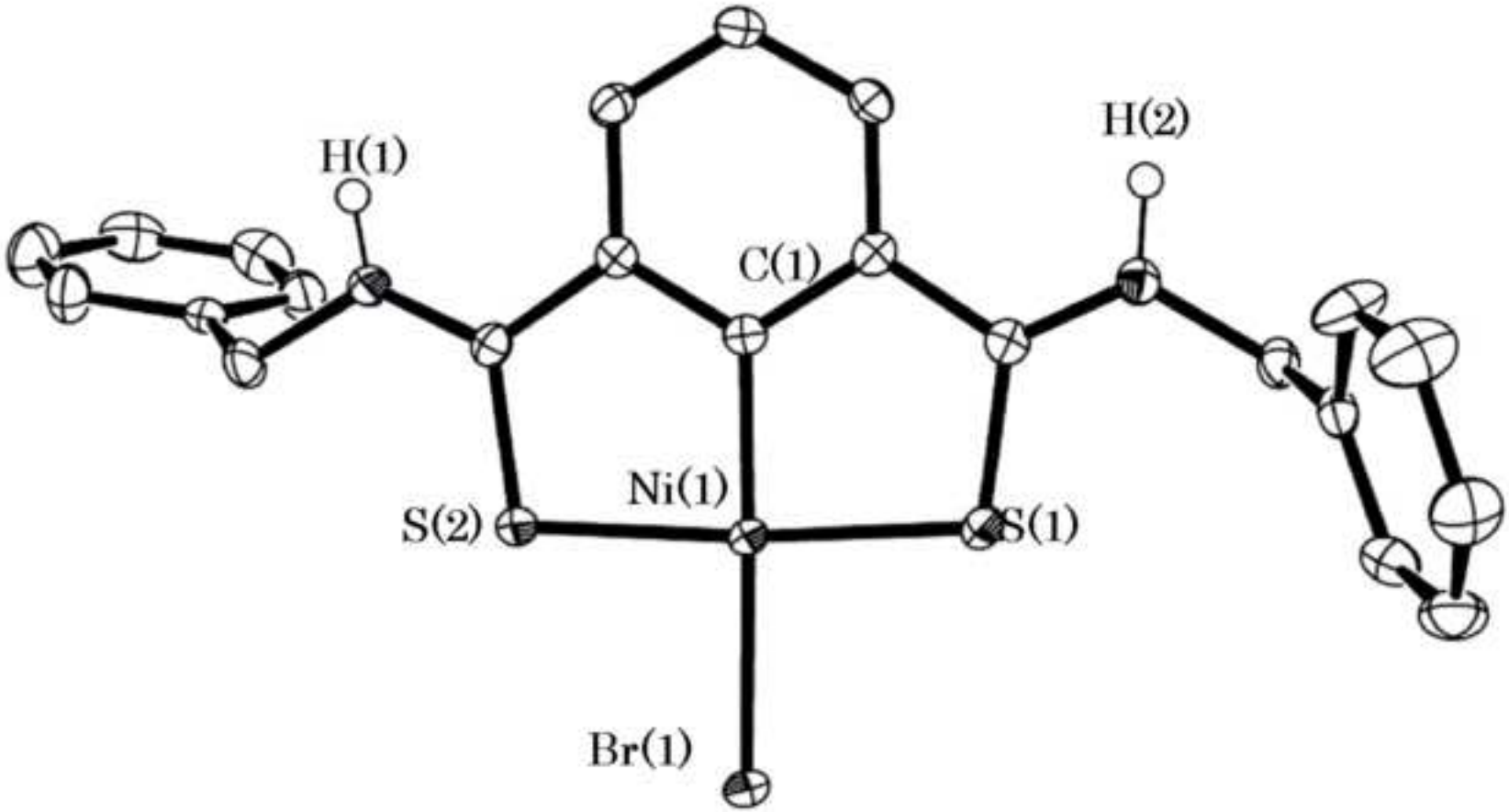

Fig. 2. ORTEP drawing of **5** DMF with 50% ellipsoidal level. Hydrogen atoms except for H1 and H2 and solvated DMF molecules are omitted for clarity.

Figure(s)
Click here to download high resolution image

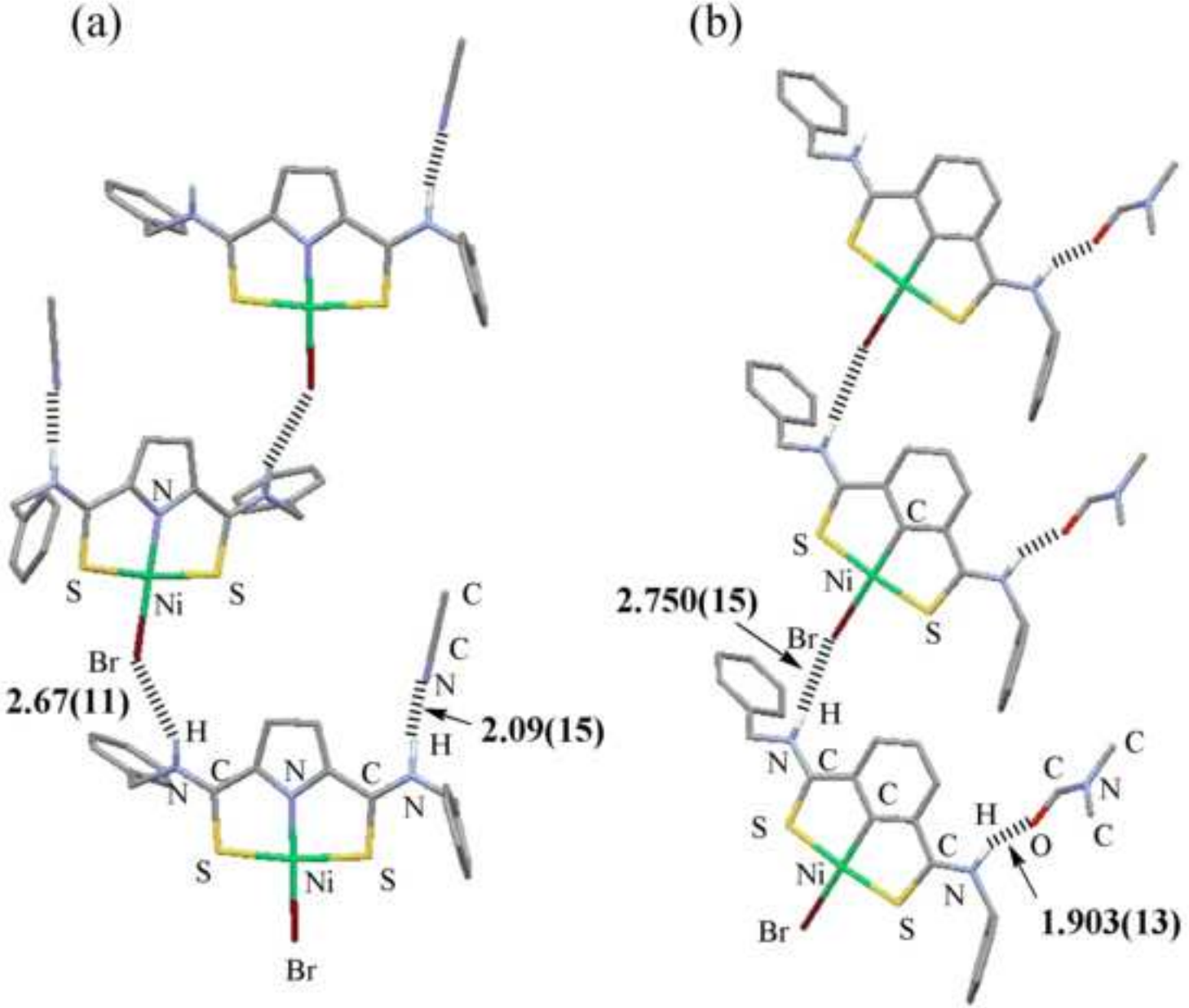

Fig. 3. Packing diagrams of (a) **2** MeCN and (b) **5** DMF.

Figure(s)
Click here to download high resolution image

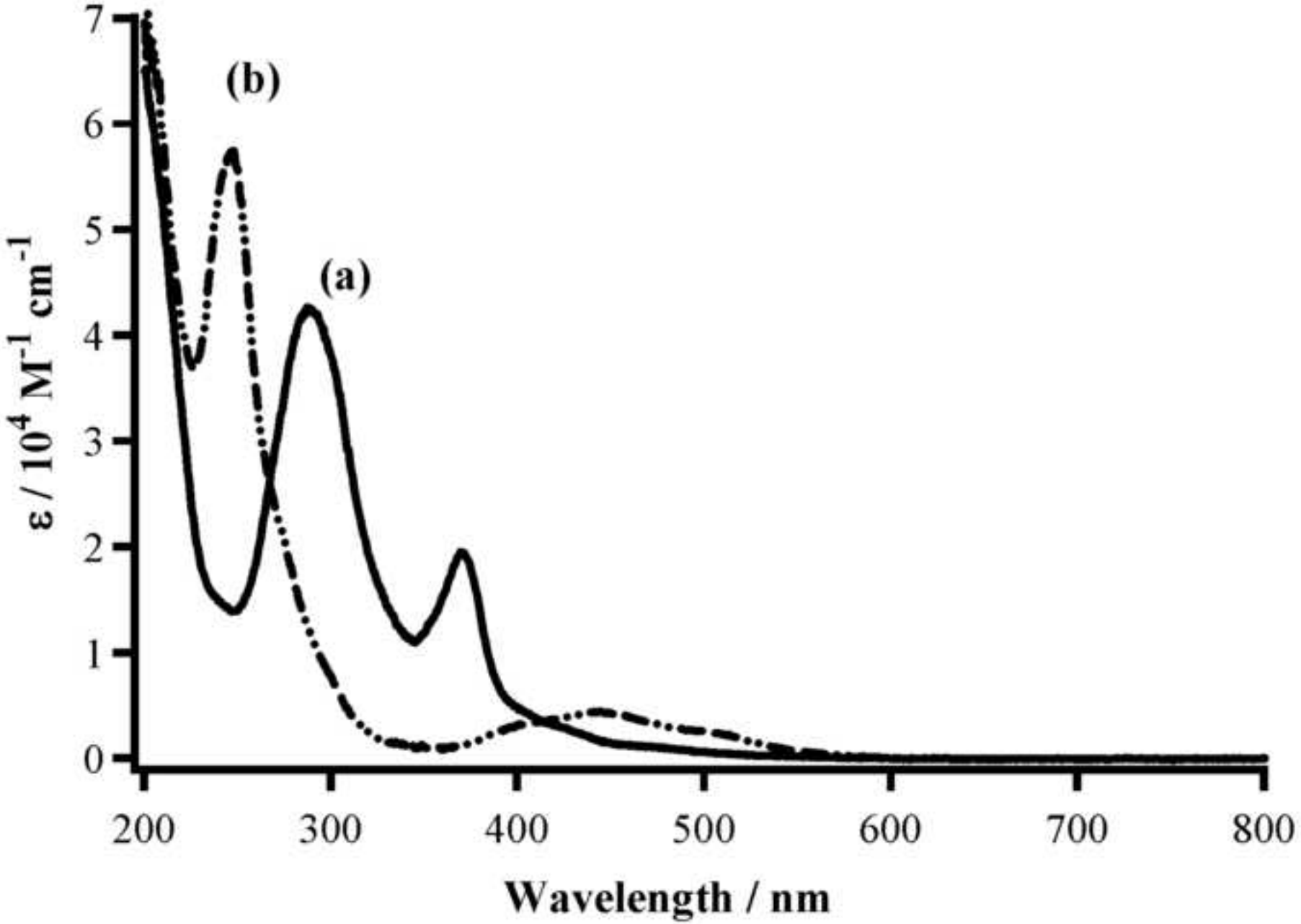

Fig. 4. Electronic spectra of (a) **2** and (b) **5** in MeCN.

Figure(s)
Click here to download high resolution image

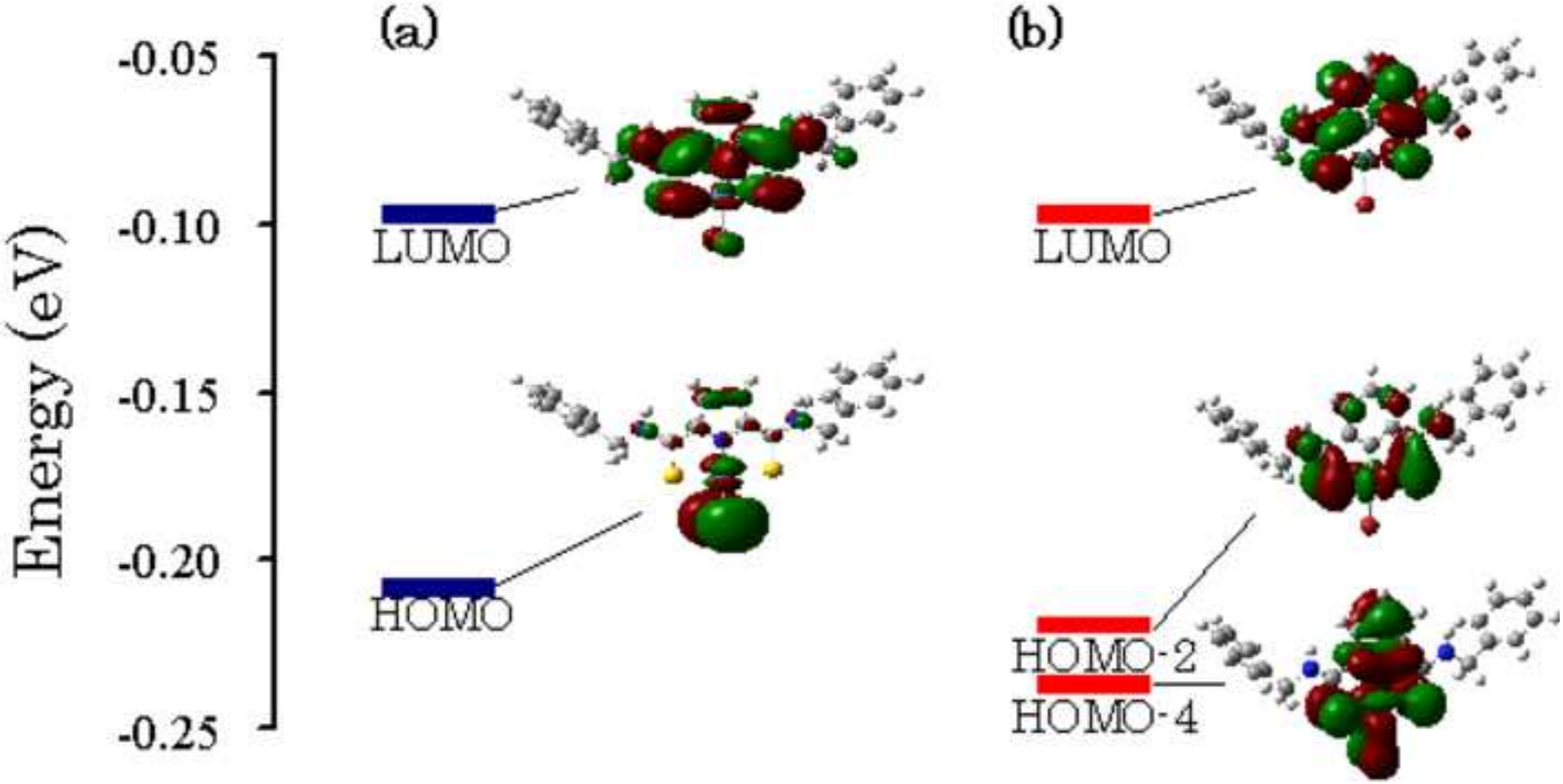

Fig. 5. Molecular orbitals (MO) and their levels of (a) **2** and (b) **5** calculated at the B3PW91/LANL2-DZ level, respectively

Figure(s)
Click here to download high resolution image

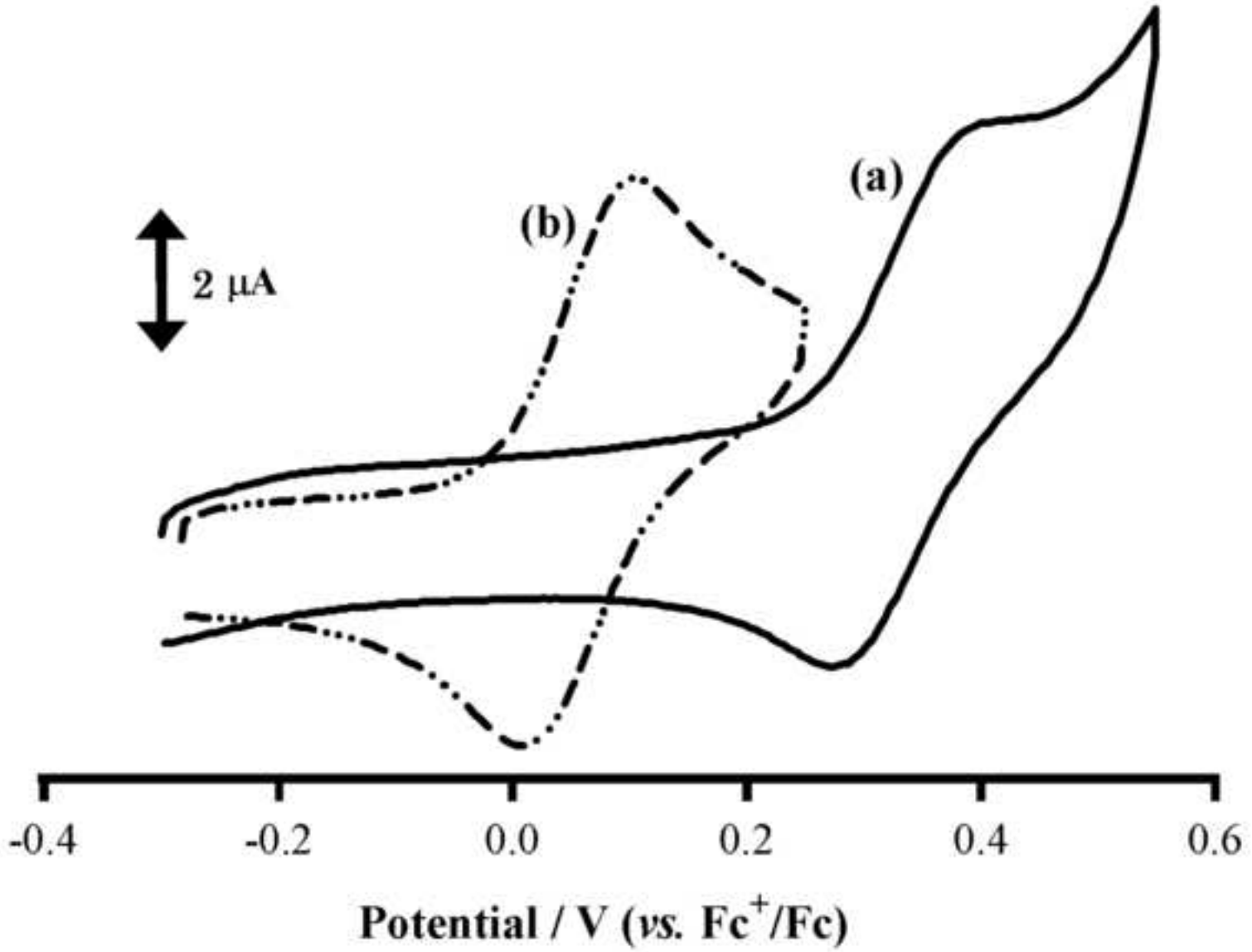

Fig. 6. Cyclic voltammograms of (a) **1** and (b) **4** in MeCN; 0.10 M $[N(n\text{-}Bu)_4]PF_6$, scan rate 50 mVs^{-1}, glassy carbon working electrode.

Figure(s)
Click here to download high resolution image

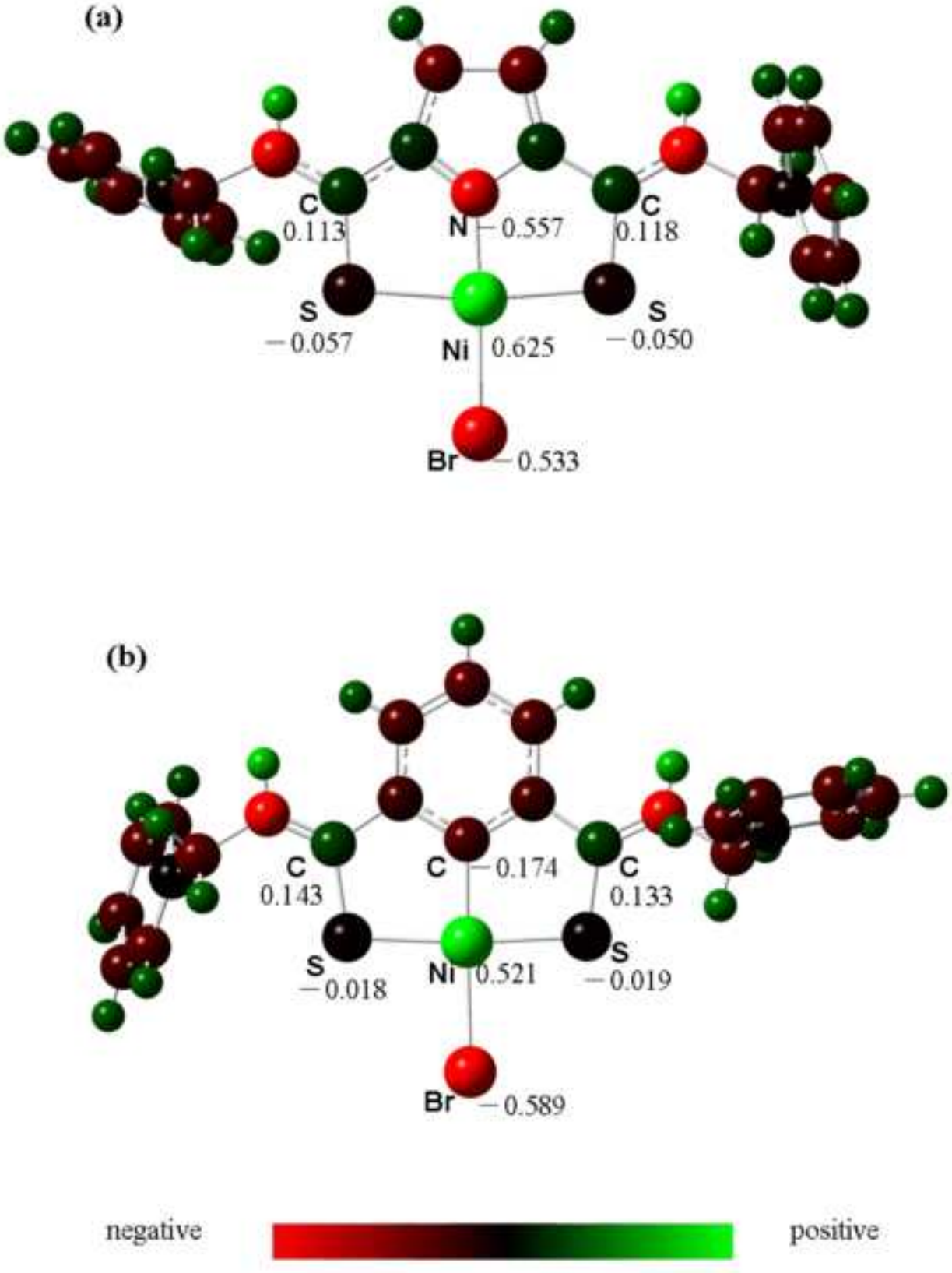

Fig. 7. Natural charge of (a) **2** and (b) **5** calculated by NPA.

Figure(s)
Click here to download high resolution image

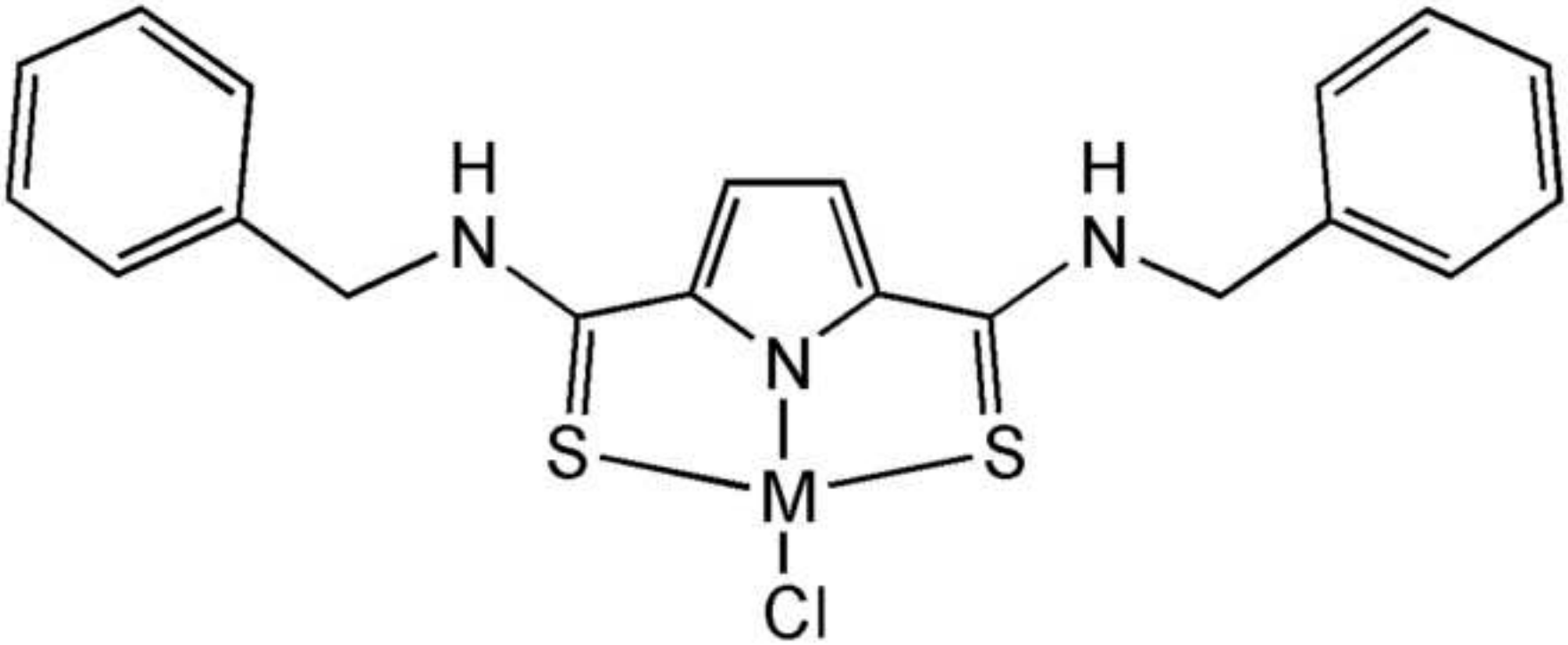

M = Ni, Pd, Pt

Scheme 1. Molecular structure of the M-(κ^3SNS) complex.

Figure(s)
Click here to download high resolution image

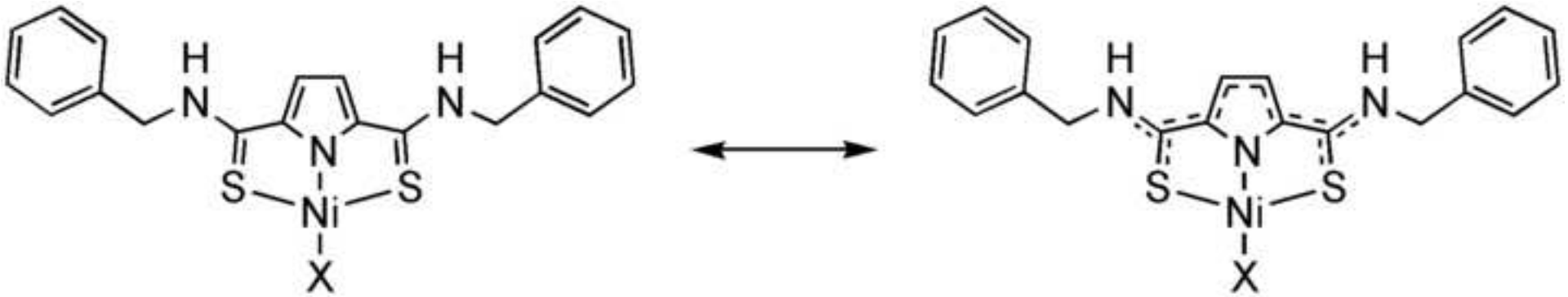

Scheme 2. Delocalization of electrons in the Ni(SNS) complex.

Figure(s)

Click here to download high resolution image

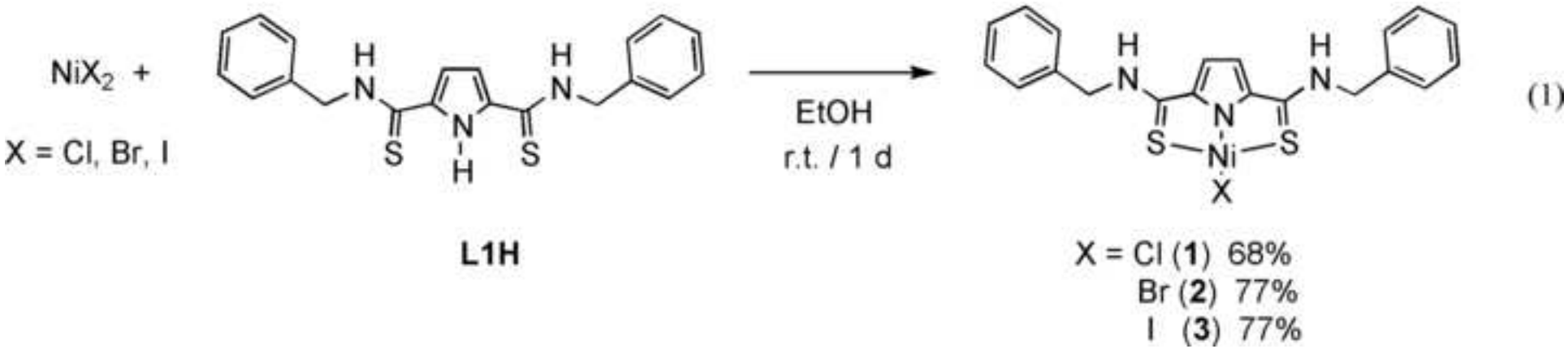

Figure(s)

Click here to download high resolution image

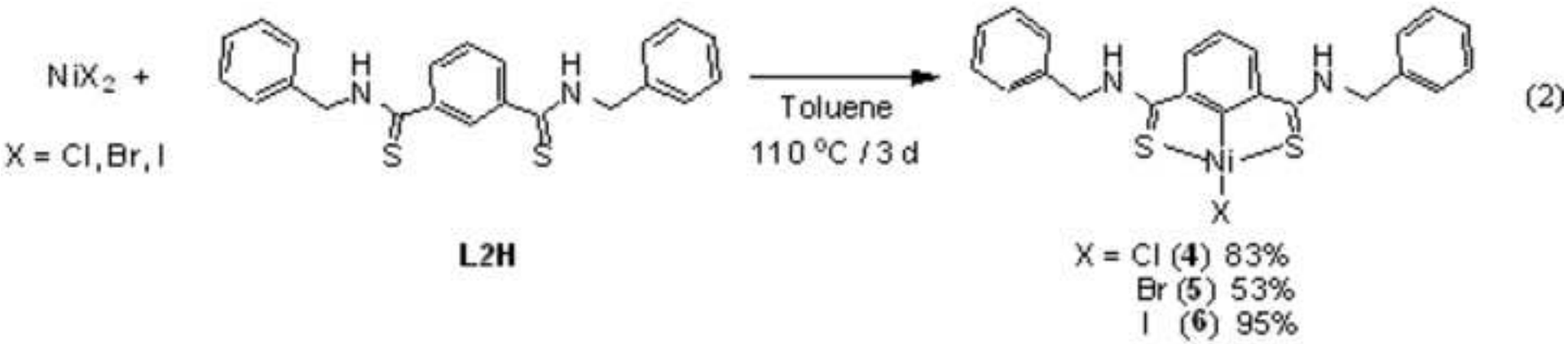

Table 1. Selected bond lengths (Å) and angles (°) of 2·MeCN.

Complex **2**			
Ni1-Br1	2.321(2)	Ni1-S1	2.229(3)
Ni1-S2	2.241(4)	Ni1-N1	1.817(12)
S1-C5	1.717(12)	S2-C13	1.703(15)
N2-C5	1.348(7)	N3-C13	1.311(6)
C1-C5	1.473(18)	C4-C13	1.43(2)
Br1-Ni1-N1	177.6(3)	Br1-Ni1-S1	94.38(11)
Br1-Ni1-S2	93.90(12)	S1-Ni1-S2	171.72(15)
S1-Ni1-N1	88.0(3)	S2-Ni1-N1	83.7(3)
Ni1-N1-C1	122.7(8)	Ni1-N1-C4	130.0(9)
N1-C1-C5	115.1(11)	N1-C4-C13	110.1(12)
S1-C5-C1	115.9(9)	S2-C13-C4	119.2(10)
Ni1-S1-C1	98.3(4)	Ni1-S2-C13	97.0(5)

Table 2. Selected bond lengths (Å) and angles (°) of 5·DMF.

Complex **5**			
Ni1-Br1	2.3686(2)	Ni1-S1	2.1735(3)
Ni1-S2	2.1757(3)	Ni1-C1	1.8630(11)
S1-C7	1.7163(12)	S2-C15	1.7034(12)
N1-C7	1.3144(15)	N2-C15	1.3203(14)
C6-C7	1.4626(15)	C2-C15	1.4614(16)
Br1-Ni1-C1	175.82(3)	Br1-Ni1-S1	94.007(10)
Br1-Ni1-S2	90.797(10)	S1-Ni1-S2	175.195(14)
S1-Ni1-C1	87.73(3)	S2-Ni1-C1	87.47(3)
Ni1-C1-C2	121.46(8)	Ni1-C1-C6	121.56(8)
C1-C6- C7	114.35(10)	C1- C2- C15	114.58(10)
S1-C7-C6	115.83(8)	S2-C15-C2	115.80(8)
Ni1-S1-C7	100.52(3)	Ni1-S2-C15	100.41(4)

Table 3. UV-vis spectral data for the complexes in MeCN.

	λ_{max} / nm (ε /L mol^{-1}cm^{-1})
1	292 (43100), 372 (16700)
2	287 (42700), 369 (9800)
3	246 (24900), 286 (43300), 369 (20200)
4	248 (64400), 452 (9000)
5	248 (57400), 444 (8800)
6	246 (69100), 440 (9250)

Table 4. Selected Calculated Singlet Excited-State Transitions for Complexes for 2 and 5.

Complex	Wavelength (nm)	Oscillator strength	Assignment (% of major transition contributing to the band)
2	506	0.0368	HOMO→LUMO (89%)
5	437	0.0724	HOMO-2→LUMO (46%)
	401	0.0654	HOMO-4→LUMO (80%)

Table 5. Electrochemical data for complexes 1-6.

	E / V (*vs*. Fc^+/Fc)		
	$[Ni]^+/[Ni]^0$	$[Ni]^{2+}/[Ni]^+$	$[Ni]^{3+}/[Ni]^{2+}$
1	E_{pa} = 0.397	E_{pa} = 0.768 (irr)	
	E_{pc} = 0.274		
2	E_{pa} = 0.464	E_{pa} = 0.847 (irr)	
	E_{pc} = 0.223		
3	E_{pa} = 0.457		
	E_{pc} =0.369		
4	E_{pa} = 0.102	E_{pa} = 0.566 (irr)	E_{pa} = 0.807 (irr)
	E_{pc} =0.008		
5	E_{pa} = 0.092	E_{pa} = 0.362 (irr)	E_{pa} = 0.787 (irr)
	E_{pc} = - 0.012		
6	E_{pa} = 0.139	E_{pa} = 0.362 (irr)	
	E_{pc} = - 0.098		

Condition: Sample: 1 mM / MeCN; Electrolyte: *n*-Bu_4NBF_4 0.1 M; Working electrode: glassy carbon; Counter electrode: Pt wire. Sweep rate: 50 mV s^{-1}.

Table 6. Crystal data and details of the structure refinement of 2·MeCN and 5·DMF.

	2·MeCN	**5·DMF**
Formula	$C_{22}H_{21}BrN_4NiS_2$	$C_{25}H_{26}BrN_3NiS_2O$
Molecular weight	544.16	587.22
Crystal system	Monoclinic	Monoclinic
Space group	$P2_1/c$ (No. 14)	$P2_1/c$ (No. 14)
a (Å)	9.084(10)	9.1750(15)
b (Å)	16.121(17)	18.545(3)
c (Å)	15.850(16)	14.721(2)
α (°)		
β (°)	103.260(5)	96.0577(9)
γ (°)		
V (Å^3)	2259(4)	2490.8(7)
Z	4	4
μ (cm^{-1})	28.265	25.790
F(000)	1016.00	1200.00
D_{calc} (g cm^{-3})	1.479	1.566
No. unique reflns	5083	5482
No. reflns used	5083	5482
No. variables	271	402
R_1[a]	0.0808	0.0253
R	0.1165	0.0315
R_w[b]	0.1878	0.0350

[a] $R_1 = \Sigma||F_o|-|F_c||/\Sigma|F_o|$ for $I > 2.0\sigma(I)$ data. [b] $R_w = \Sigma[w(F_o^2-F_c^2)^2/\Sigma w(F_o^2)^2]^{1/2}$. [c] Weighting scheme $1/[0.0159F_o^2+1.0000\sigma(F_o^2)]$. [d] Weighting scheme $1/[0.0005F_o^2+1.0000\sigma(F_o^2)]$.

CIF Data Files (if paper contains X-ray crystal structures)

Click here to download CIF Data Files (if paper contains X-ray crystal structures): CIF_complex-2.cif

CIF Data Files (if paper contains X-ray crystal structures)

Click here to download CIF Data Files (if paper contains X-ray crystal structures): CIF_complex-5.cif

CIF Data Files Validation Report (if paper contains X-ray crystal structures)

Click here to download CIF Data Files Validation Report (if paper contains X-ray crystal structures): checkcif_complex-2.pdf

CIF Data Files Validation Report (if paper contains X-ray crystal structures)

Click here to download CIF Data Files Validation Report (if paper contains X-ray crystal structures): checkcif_complex-5.pdf